5

High performance analog optical links based on quantum dot devices for UWB signal transmission

M. Ran, Y. Ben Ezra and B.I. Lembrikov
Holon Institute of Technology (HIT),
P.O.Box 305, 58102, 52 Golomb Str., Holon
Israel

1. Introduction

In this chapter, we discuss the possibility of quantum dot (QD) laser and QD semiconductor optical amplifier (SOA) applications in ultra-wideband (UWB) communication systems. We mainly concentrate on novel methods of UWB pulse photonic generation, UWB over optical fiber (UROOF) technology, and in particular, performance of analogous optical links in UROOF systems. We demonstrate that QD devices are promising candidates for different applications in the communication systems due to their low bias current, high temperature stability, extremely high operation rate, and the possibility of the light generation in a wide range of optical frequencies. We briefly discuss the state-of-the-art in UWB technology and present original results concerning UWB pulse photonic generation based on passive elements, and application of a QD laser in an analogous optical link.
The chapter is constructed as follows. In Section 2, we discuss the UWB communication state-of-the-art. In Section 3, we discuss the photonic generation of the UWB pulses and present original experimental results concerning the generation of UWB Gaussian pulses with passive elements. In Section 4, we describe the novel approach to UWB communication systems known as UROOF technology which permits to increase dramatically the distance of the UWB signal transmission and to improve the UWB system performance. In Section 5, we analyze the structure and performance of an analog optical link as a key element of the UROOF communication system. The improvement of the analog optical link performance, especially with respect to operation rate and bandwidth, can be achieved by implementation of integrated photonic and electronic circuits. The possibilities of Si photonics applications in UROOF technology are discussed in Section 6. The key element of UROOF communication system is a laser diode as a source of a directly modulated optical carrier. The structure, operation principle and dynamics of QD lasers are discussed in Section 7. We have carried out numerical simulations for the analogous optical link with the QD laser instead of a conventional vertical cavity surface emitting laser (VCSEL) using the coupled rate equations. The theoretical results predict a high performance of such a link. Conclusions are presented in Section 8.

2. UWB Communications

UWB radar systems were developed primarily for radar and military applications Ghawami (2005), Chong (2006). Recently, UWB technology has been focused on consumer electronics and communications Ghawami (2005). Possible UWB communication system applications include radars, wireless personal area networks (WPAN), sensor networks, imaging systems, UWB positioning systems, etc. Yang (2004), Kshetrimayum (2009). UWB transmission is characterized by high data rate, availability of low-cost transceivers, low transmit power, and low interference Ghawami (2005), Qui (2006). UWB systems have low power spectral density (PSD), and consequently can coexist with cellular systems, wireless local area networks (WLAN), global positioning systems (GPS) etc. Chong (2006). UWB operate at the noise level or even below it, and for this reason they are inherently covert and difficult for unintended users to detect Chong (2006).
The three main types of UWB technologies are following Ran (2009).

1. Impulse radio (IR-UWB).
2. Direct sequence (DS-UWB).
3. Multi-band orthogonal frequency division multiplexing (MB-OFDM).

In IR-UWB, information is carried by a set of narrow electromagnetic pulses with bandwidth inversely proportional to the pulse width. The center frequency in IR-UWB is determined by the zero crossing rate of the pulse waveform. Various data modulation format (DMFs) may be used in the case of IR-UWB such as pulse amplitude modulation (PAM), pulse position modulation (PPM) and pulse shape modulation (PSM). DS-UWB is based on concepts of conventional DS spread spectrum (DS-SS). MB-OFDM is based on subdividing the UWB spectrum into 5 band groups and 14 sub-bands of $528MHz$ width composed of 128 sub-carriers OFDM modulated signals. The MB UWB OFDM technology combines the advantages of spectral efficiency (SE) DMFs and OFDM. OFDM has emerged as the leading physical-layer interface in broadband wireless communication systems because it is characterized by a comparatively low intersymbol interference (ISI), and it transfers the complexity of transmitters and receivers from the analog to the digital domain Shieh (2008), Armstrong (2009). In OFDM the spectra of individual subcarriers overlap, but for linear channels the subcarriers can be demodulated without interference and without an analog filtering to separate the received subcarriers Armstrong (2009). Optical OFDM has been proposed which is based on electronic signal processing before the optical modulator and after the photo detector (PD) Shieh (2008).
UWB signals are based on short pulses rather than the harmonic sine waves Qui (2006). UWB can be described as baseband, carrier-free and impulse technology Ghawami (2005). The extremely short UWB pulses can be distinguished from unwanted multipath reflections which leads to the multipath immunity; UWB pulses' low frequency components enable the signals propagate through materials; extremely high data rates can be achieved due to the large bandwidth; UWB transmitters and receivers are compact, low-cost, have low power consumption as compared to conventional narrow-band communication systems; they do not require expensive and large modulators and demodulators Ghawami (2005). According to the Federal Communications Commission (FCC) decision, the unlicensed frequency band between 3.1 and $10.6GHz$ is reserved for indoor UWB wireless communication systems Qui (2006). It is seen from the well known Shannon's capacity equation

$$C = B \log \left(1 + \frac{S}{N}\right) \tag{1}$$

that UWB systems have a great potential for high-capacity wireless communications Ghawami (2005). Here C is the maximum channel capacity in $bits/s$, B is the channel bandwidth, in Hz, S is the signal power, in $watts$, and N is the noise power, in $watts$. PSD of UWB is defined as $PSD = P/B$ where P is the transmitted power in watts Ghawami (2005). It is very low compared to conventional systems due to a very large bandwidth B. For instance, for UWB power $P = 1mW$, we obtain $PSD = 0.013W/MHz$ Ghawami (2005).
After transmission, an electromagnetic signal travels by various paths to the receiver which is called a multipath phenomenon Ghawami (2005). It is caused by the physical effects such as reflection, absorption, diffraction, and scattering, and leads, in particular, to ISI and a time delay Ghawami (2005). The multipath interference can be diminished by decreasing the pulse width, or by increasing the time delay between pulses, i.e. by decreasing the duty cycle of the system Ghawami (2005). UWB systems are immune to multipath fading and capable of resolving multipath components (MPCs) in dense multipath environments Chong (2006). Gaussian monocycle and doublet pulses provide better multipath performance among other impulse signals Yao (2009). However, it is difficult and expensive to generate such pulses with a fractional bandwidth greater than 100% at the central frequency of about $7GHz$ Yao (2007). The penetration capabilities of UWB are determined by the lower frequency components of about $1GHz$, and they have substantially decreased due to the increase of the UWB lower frequency limit up to $3.1GHz$ Ghawami (2005). They can operate under both line-of-sight (LOS) and non-LOS conditions Chong (2006). UWB applications are targeting the data rate up to $500Mbps$ that is much larger than the bit rate of Bluetooth, or the wireless local area network (WLAN) standards Ghawami (2005), Qui (2006). Low complexity and consequently low cost of UWB technology are determined by nearly "all-digital" structure of UWB systems Ghawami (2005), Qui (2006). They can be implemented on a single chip architecture Chong (2006). However, the UWB communication distances are limited by less than $10m$ due the FCC constraints on allowed emission levels Ran (2009). In order to increase the area of coverage a novel approach based on the UROOF technology has been recently proposed Ran (2009), Yao (2009). The state-of-the-art optical fibers possess low loss and broad bandwidth, and for this reason the UROOF technology is a promising solution Ran (2009), Yao (2009). In order to distribute UWB signals over the optical fiber, it is desirable to generate these signals directly in the optical domain without extra electrical-to-optical (E/O) conversion Yao (2007), Yao (2009).

3. Photonic Generation of UWB Pulses

UWB pulses are of nanosecond or picosecond order, with a typical pulse shape approximating a Gaussian function y_{g1}, a Gaussian monocycle y_{g2} and a Gaussian doublet y_{g3} given by the first and the second derivative of a Gaussian pulse, respectively Ghawami (2005)

$$y_{g1} = K_1 \exp\left(-\frac{t^2}{\tau^2}\right) \tag{2}$$

$$y_{g2} = K_2 \left(-\frac{2t}{\tau^2}\right) \exp\left(-\frac{t^2}{\tau^2}\right);\ y_{g3} = K_3 \left(-\frac{2}{\tau^2}\right)\left(1 - \frac{2t^2}{\tau^2}\right) \exp\left(-\frac{t^2}{\tau^2}\right) \tag{3}$$

where $-\infty < t < \infty$, τ is the time-scaling factor, and $K_{1,2,3}$ are normalization constants. Gaussian pulses are the most widely used waveforms due to their simplicity and feasibility Yao (2007). The important property of the Gaussian pulses (2), (3) is that they are almost uniformly distributed over their frequency spectrum Ghawami (2005).

A number of optically based methods of the Gaussian IR UWB monocycles and doublets generation for low-cost high-data rate UWB wireless systems have been proposed Lin (2005), Le Guennec (2007), Yao (2007), Zeng (April 2006), Zeng (October 2006), Zeng (2007), Ben Ezra (2008). The advantages of these methods are following: the decreasing of interference between electrical devices, low loss and light weight of optical fibers Lin (2005), Yao (2007), Wang (2006). The all-optical methods of IR UWB generation have been reviewed in detail Yao (2007), Ben Ezra (2009). In particular, we concentrated on the all-optical methods of UWB pulse generation based on cross phase modulation (XPM) and cross gain modulation (XGM) in SOAs. We proposed a theoretical analysis of a novel all-optical method of the IR UWB pulse generation in an integrated Mach-Zehnder interferometer (MZI) with QD SOA as an active element inserted into one arm of the integrated MZI which results in an intensity dependent optical signal interference at the output of MZI Ben Ezra (2008).
Recently, a novel method of photonic passive generation of UWB pulse in the form of the Mexican hat mother wavelet (MHMW) proportional to the Gaussian doublet Rao (1998) has been proposed based on the system of two unbalanced Mach-Zehnder Interferometers (UMZIs) connected in parallel that does not contain any active elements Ben Ezra (June 2009). The proposed method provides the pulse shaping directly in the time domain and does not require additional optical filters and FBG. The block diagram of the UMZIs connected in parallel is shown in Fig. 1. The UMZIs are chosen in such a way that the phase difference of the interfering signals at the output is equal to π. As a result, at the output of the UMZIs the interfering optical signals modulated by a Gaussian UWB pulse form the first-order difference approximating the Gaussian monocycle and the second-order difference approximating the Gaussian doublet. At the output of the system, the UWB monocycles and doublets can be converted to a UWB signal by means of a homodyne detection where the local oscillator frequency ω_{LO} coincides with the optical carrier frequency ω Agrawal (2002). In such a case the homodyne detected signal is proportional to the UWB modulated optical signal amplitude Agrawal (2002), i.e. to the Gaussian monocycle or doublet in our case.

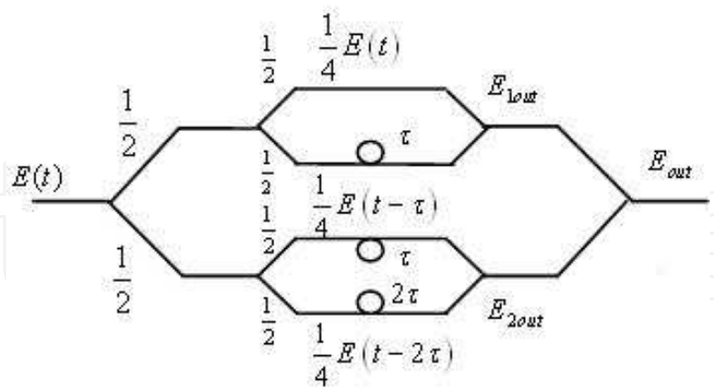

Fig. 1. The UMZIs connected in parallel

The UWB modulated optical carrier field $E(t) = A(t)\exp[-i(\omega t + \phi)]$ is split in the two equal parts at the input of the system, and then the each signal is split equally once more at the input of the both UMZIs. Here $A(t), \phi$ are the amplitude and phase of the input signal, respectively. Assuming the delay time τ of the lower arm of the upper UMZI1 and of the upper arm of the lower UMZI2 and the delay time 2τ of the lower arm of the lower UMZI2 we can describe the interfering optical fields as follows.

$$E_{1,2in} = \frac{1}{2}E(t); E_{1up} = \frac{1}{4}E(t); E_{1low} = \frac{1}{4}E(t-\tau) \tag{4}$$

$$E_{2up} = \frac{1}{4}E(t-\tau); E_{2low} = \frac{1}{4}E(t-2\tau) \tag{5}$$

$$E_{1out} = E_{1up} - E_{1low} = \frac{1}{4}[E(t) - E(t-\tau)] \tag{6}$$

$$E_{2out} = E_{2up} - E_{2low} = \frac{1}{4}[E(t-\tau) - E(t-2\tau)] \tag{7}$$

$$E_{out} = E_{1out} - E_{2out} = \frac{1}{4}[E(t) - 2E(t-\tau) + E(t-2\tau)] \tag{8}$$

It is easy to see from eqs. (6)-(8) that the output fields E_{1out}, E_{2out} of the UMZI1 and UMZI2, respectively, correspond to the first-order difference of the input signal $E(t)$, and the system output signal $E_{out}(t)$ corresponds to the second-order difference of $E(t)$ which represent the approximations of the first and second derivative of $E(t)$, respectively Yao (2007). Similarly, in the case of the UMZIs connected in cascade shown in Fig. 2 we have for the interfering fields at the outputs of the UMZI1 and UMZI2.

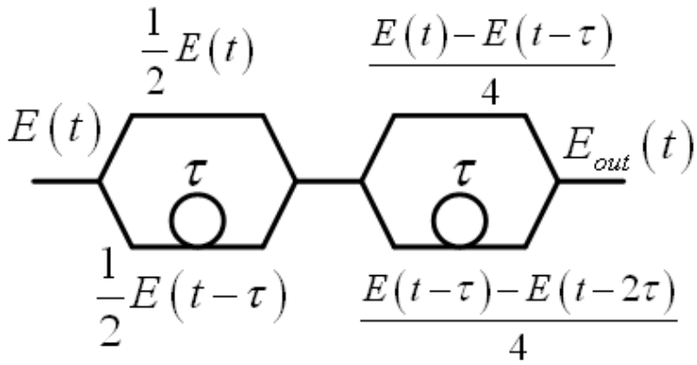

Fig. 2. The UMZIs connected in a cascade

$$E_{1,2in} = \frac{1}{2}E(t); E_{1up} = \frac{1}{2}E(t); E_{1low} = \frac{1}{2}E(t-\tau) \tag{9}$$

$$E_{1out} = E_{1up} - E_{1low} = \frac{1}{2}[E(t) - E(t-\tau)] \tag{10}$$

$$E_{2up} = \frac{E(t) - E(t-\tau)}{4}; E_{2low} = \frac{E(t-\tau) - E(t-2\tau)}{4} \tag{11}$$

and expression (8), respectively. Evidently, in the both cases the output fields correspond to the Gaussian monocycles and doublets. The system can be made tunable by including into UMZIs a tunable delay line.

In order to down-convert the output monocycle and doublet modulated optical signals, the coherent-detection technique is used where the local oscillator frequency $\omega_{LO} = \omega$ Agrawal (2002). In order to improve the accuracy of the homodyne detection we use the same laser as a source of the externally UWB modulated optical signal and the continuous wave (CW) optical signal. The detector photocurrent $I(t)$ is given by Agrawal (2002)

$$I(t) = R(P_{out} + P_{LO}) + 2R\sqrt{P_{out}P_{LO}}\cos(\phi_{out} - \phi_{LO}) \tag{12}$$

where R is the detector responsivity, $P_{out} = KA_{out}^2$, $P_{LO} = KA_{LO}^2$, A_{out}, A_{LO}, ϕ_{out}, ϕ_{LO} are the output signal and local oscillator optical powers, amplitudes and phases, respectively, K is a constant of proportionality. The phase difference $\phi_{out} - \phi_{LO}$ can be eliminated by using a phase shifter. Then, the homodyne signal is given by Agrawal (2002)

$$I_h(t) = 2R\sqrt{P_{out}P_{LO}} = 2R\sqrt{KP_{LO}}A_{out}(t) \sim |E_{out}| \tag{13}$$

Eq. (13) shows that the homodyne signal is proportional to the Gaussian doublet. Obviously, down-conversion of the output signals of MZI1 or MZI2 yields the homodyne signal proportional to the Gaussian monocycle. Typically, the local oscillator power is much larger than the output signal, and optical losses in the MZI system can be neglected: $P_{LO} \gg P_{out} \sim |A(t)|^2$. For the typical values of $R = (0.4 - 0.9)\, A/W$ Agrawal (2002), $P_{LO} = 10mW$, $P_{out} = 0.1mW$ we obtain $I_h(t)_{\max} \approx (0.8 - 1.8)\, mA$.

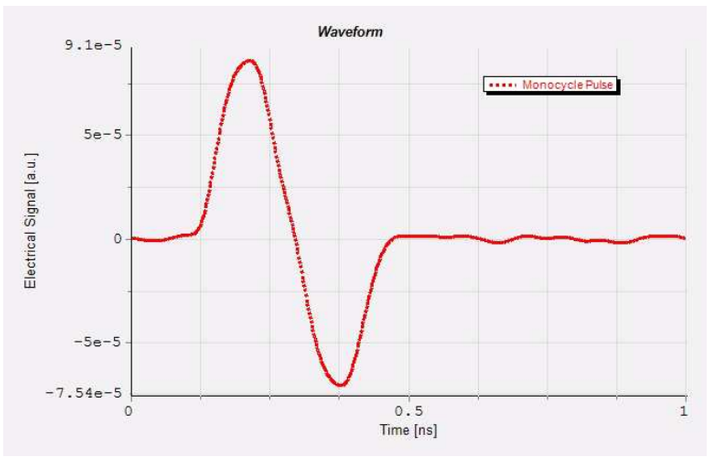

Fig. 3. Simulation results for the Gaussian monocycle at the output of the passive UMZI system

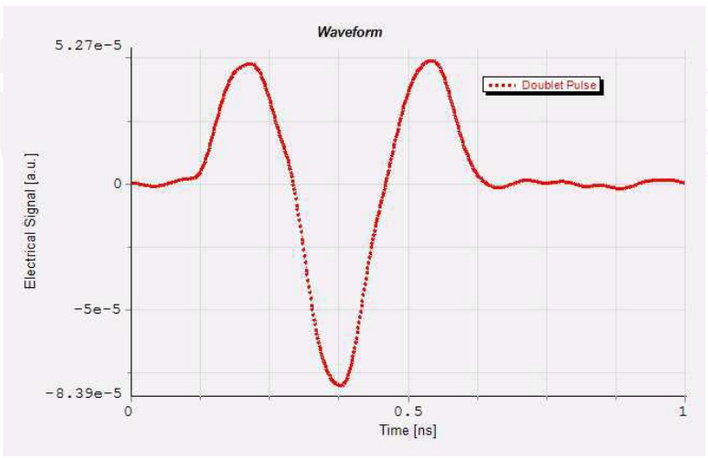

Fig. 4. Simulation results for the Gaussian doublet at the output of the passive UMZI system

The Gaussian monocycle and doublet obtained by using numerical simulations based on eqs. (4)-(8) and eqs. (9)-(11) are shown in Figs. 3, 4. The Gaussian doublet shown in Fig. 4 is generated at the output of the UMZI system as a result of the monocycle interference and further coherent homodyne detection. We have used the following data: the time window is $6.4 \times 10^{-9}s$, the sample mode bandwidth is $1.28THz$, the carrier sample mode frequency is $193.1THz$, the sampling rate is $160 \times 10^{9}Hz$, the impulse bit rate $10Gb/s$, the delay time of the optical delay line is $166ps$.
We have carried out experimentally the generation of the UWB monocycles and doublets for the case of the UMZIs connected in cascade. Block diagram of the experimental setup is shown in Fig. 5.

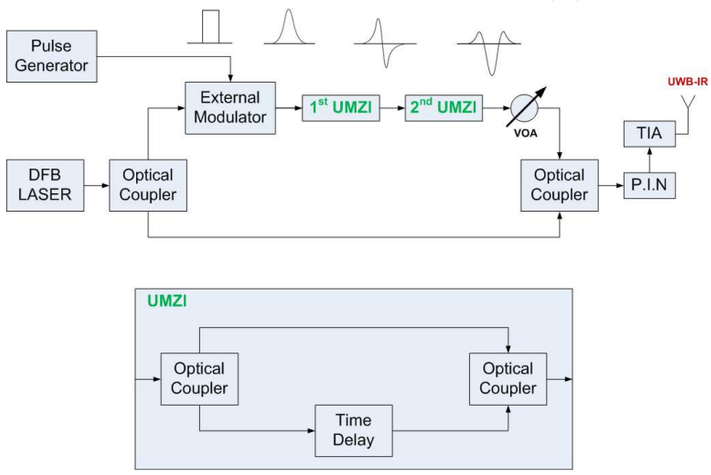

Fig. 5. Block diagram of the experimental setup for the photonic generation of UWB Gaussian monocycles and doublets

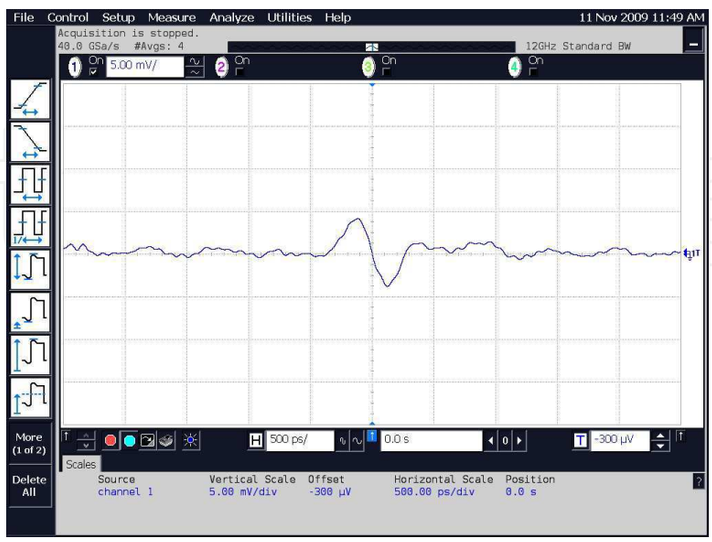

Fig. 6. The measured Gaussian monocycle at the output of UMZI1

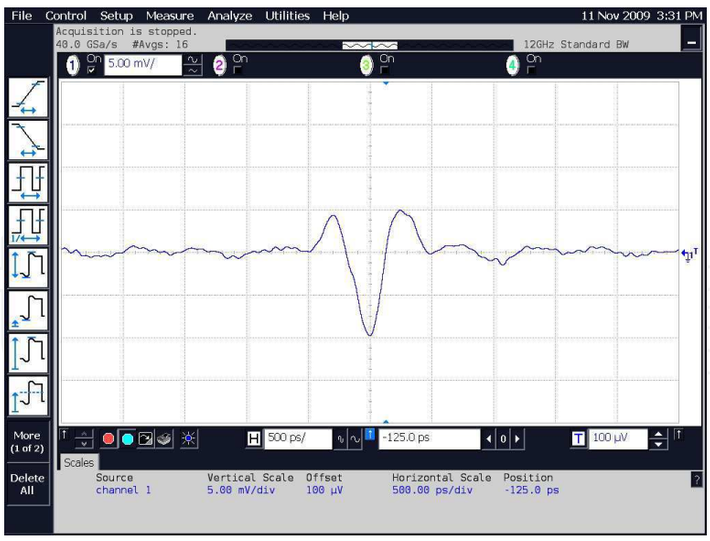

Fig. 7. The measured Gaussian doublet at the output of the passive UMZI system

It consists of the following components: $1550nm$ distributed feedback (DFB) coaxial laser, $10Gb/s$ amplitude modulator, single mode wideband optical couplers (OCs), analog PIN detector, a monolithic broadband amplifier GALI 39+, 50Ω, DC to $7GHz$, a variable optical attenuator, and connecting single mode fibers (SMFs). The UWB modulated optical signal from the laser is fed into a MZM after the OC. Electrical pulses of a fixed pattern, corresponding to one "1" every 128 bits with a bit rate of $10GHz$, in such a way that the repetition rate is $78.125MHz$ come from a pulse pattern generator Anritsu MP1763B driving the MZM. Full-width at half-maximum (FWHM) of the optical pulse is $\tau = 100ps$.

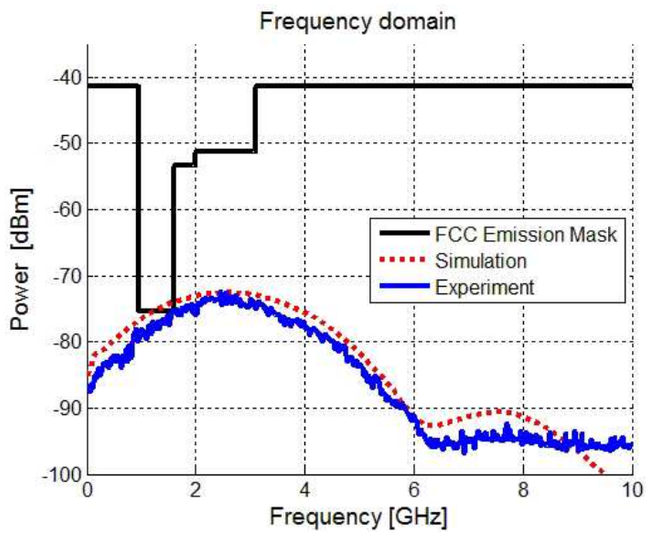

Fig. 8. Spectrum of the Gaussian monocycle: simulation results (dashed line) and experimental results (solid line)

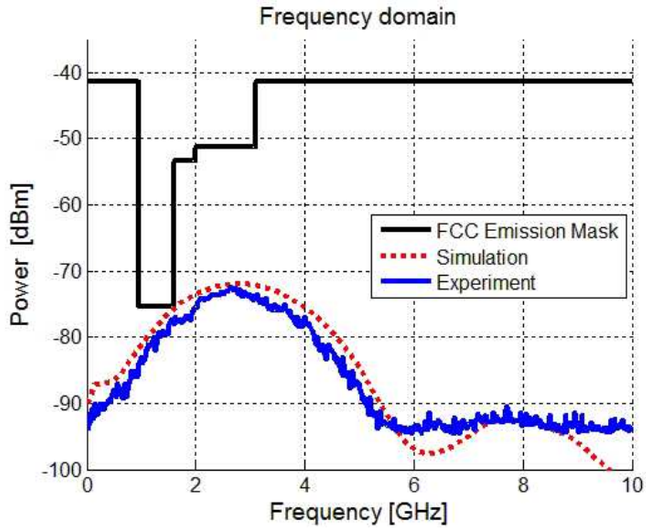

Fig. 9. The spectrum of the Gaussian doublet: the simulation results (dashed line) and the experimental results (solid line)

The measured Gaussian monocycle and doublet are shown in Figs. 6, 7. The simulation results together with the experimental results for the monocycle and doublet spectrum evaluated by using of the fast Fourier transform (FFT) are shown in Figs. 8, 9. The spectrum is limited by the FCC spectral mask. The simulation and experimental results are in a good accord as it is seen from Figs. 3, 4, 6-9.
Recently, self-organized In(Ga)As/Ga(Al)As QD lasers grown directly on Si have been demonstrated Mi (2009). In the framework of an integrated all-optical signal processing system, such an externally or directly modulated QD laser can be used as a source of UWB modulated optical carriers. Integrated UMZIs based on Si waveguides can then generate UWB Gaussian monocycles and doublets.

4. UWB over Optical Fiber (UROOF) Technology

Fiber-optic communication systems use carrier frequencies in the visible or near-infrared region of the electromagnetic radiation spectrum, i.e. about 10^{14} Hz, and can be applied for the information transfer from one place to another. Fiber-optic communications have the following advantages Agrawal (2002):

1. Extremely low fiber losses exhibiting a minimum loss of about $0.2 dB/km$ near the wavelength $\lambda = 1.55 \mu m$
2. Compatibility with semiconductor lasers and SOAs.
3. The possibility of operation as Erbium doped fiber amplifier (EDFA), or Raman fiber amplifier.
4. High bit rate of information transmission.
5. Large transmission distances.
6. The possibility of a system capacity increase by virtue of OFDM technology.
7. Soliton communications.

Fiber-optic communication system can be divided into three groups: (i) point-to-point links; (ii) distribution networks; (iii) local area networks (LAN) Agrawal (2002). In particular, the UROOF concept enables the transmission of UWB radio frequency (RF) signals over optical fibers by superimposing the UWB RF signals of several GHz on the optical CW carrier Ran (2009), Yao (2009). UROOF applications are related to the short-haul case Ran (2009). UROOF technology can be successfully applied in WPAN, security systems with a large number of sensors and cameras equipped with UWB, and broadband multimedia Ran (2009). In a typical application of a broadband indoor system, UWB signals are generated and encoded in a central office and distributed over optical fiber to the access points where the UWB signals are down-converted from the optical domain to the electrical domain and the detected UWB signals radiate to free space Ran (2009), Yao (2009). UROOF technology has the following advantages Ran (2009), Yao (2009):

1. The conversion process becomes transparent to the UWB modulation method.
2. The high costs of additional electronic components required for synchronization and other processes can be avoided.
3. The integration of all the RF and optical transmitter/receiver components on a single chip is possible.

For the sake of definiteness, we consider the analog optical communication systems which permit the transmission of multilevel modulated radio signals as an envelope of the optical carrier over the optical fiber Ran (2009).

5. UWB Analog Optical Link

In this section we briefly discuss the problems related to the high-performance optical links in UROOF communication systems. UWB high-speed optical link includes E/O converter, an optical fiber, and optical/electrical (O/E) converter Ran (2009). We need to carry out the modulation of an optical signal, or up-conversion, at the input of the UROOF system, and separation of the electrical signal envelope from the optical carrier, or down-conversion (detection), at the output of the UROOF system Ran (2009). After the O/E conversion, a conventional radio receiver can be used for the further detection of a multilevel modulated signal Ran (2009). The optical link block diagram is shown in Fig. 10.

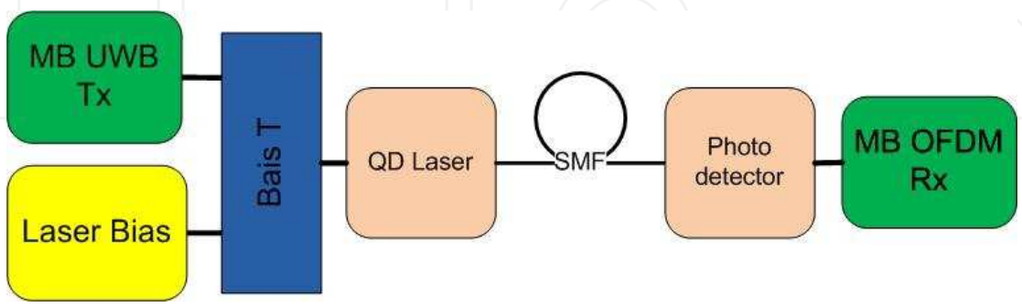

Fig. 10. Block diagram of the optical link. MB UWB Tx - transmitter, MB UWB Rx -receiver, SMF - single mode fiber

During E/O conversion process, UWB analog signals are imparted onto the optical carrier via an optical modulation device where any parameter of the optical carrier can be modulated

such as intensity, phase, frequency, or polarization. The intensity modulation is commonly used in analog optical links. There are two main methods of optical carrier intensity modulation: direct modulation and external modulation. In the first case, the analog UWB signal modulates the intensity of the diode laser which possesses a sufficient bandwidth; in the second case, the laser operates in a CW regime and the intensity modulation is imposed via an external device Cox (2003). A directly modulated link combines a diode laser with a photodiode detector Cox (2003). External modulation is usually realized by MZI fabricated in electro-optic crystal $LiNbO_3$, and an externally modulated link combines a CW laser, MZI modulator and a photodiode Cox (2003).
The performance of the analog optical link is characterized by three most common and basic parameters: the intrinsic link gain, noise figure (NF), and intermodulation-free dynamic range (IMFDR) Cox (2003). These parameters are defined as follows Cox (2003). The intrinsic link gain g_i (without any amplifiers) is defined as the available power gain between the input to the modulation device and the output of the photodetection device. NF specific for the modulation links has the form.

$$NF\,(dB) = 10\log\left[\frac{(S/N)_{in}}{(S/N)_{out}}\right] = 10\log\left(\frac{N_{out}}{kTg_i}\right) \tag{14}$$

where $(S/N)_{in}$, $(S/N)_{out}$ are signal-to-noise ratio (SNR) at the input and output, respectively, T is the temperature in K, the input noise N_{in} is taken as thermal noise at $T = 290K$,

$$N_{out} = g_i N_{in} + N_{link} \tag{15}$$

and the link noise N_{link} consists of the sum of laser relative intensity noise (RIN) and thermal noise of the modulation and photodetection devices. The IMFDR is defined as the SNR for which the non-linear distortion terms are equal to the noise floor. The two most common IMFDRs are the second- and third-order non-linear distortions Cox (2003). The advantages of the direct modulation are the simplicity and low cost. The most promising laser diodes for the direct modulation in UROOF optical links are low cost, compact, easily packaged VCSELs Ran (2009). The low level of RIN and coupling losses can be achieved in the case of a single-mode VCSEL. However, the VCSEL performance in analog communication systems is significantly lower than in digital ones Ran (2009). For instance, the strong nonlinearity in VCSELs gives rise to IMFDR related mainly to the third order intermodulation which results in the dynamic range limitation. For this reason, lasers with better performance are needed. In the following sections we consider QD lasers as promising candidates for the improvement of the optical link performance.

6. Possible Si Photonics Applications in UROOF Technology

The existing UROOF systems are relatively large and expensive since they are based on discrete photonic and microwave components made from III-V based compounds such as GaAs, InP, or the electro-optic crystal $LiNbO_3$ Reed (2004), Yao (2009). In order to reduce size and lower the cost of the components, it is necessary to develop novel O/E and E/O components and subsystems for the UROOF based on Si photonic integrated circuits (PICs) Yao (2009). Generally, the Si photonics development is crucial for UROOF system performance improvement. The advantages of the Si photonics are the compatibility with the silicon manufacturing, low cost, the highest crystal quality, the strong optical confinement, the possibility of strongly pronounced nonlinear optical effects, high-quality silicon-on-insulator (SOI) wafers serving

as an ideal platform for planar waveguide circuits Jalali (2006). Silicon photonics may provide such devices as integrated transceivers for synchronous optical networks, optical attenuators, optical interconnects for CMOS electronics, photonic crystals, waveguide-to-waveguide couplers, Mach-Zehnder interferometers, arrayed waveguide gratings (AWG), etc. Reed (2004), Jalali (2006). The principal goal of electronic and photonic integrated circuits (EPIC) development is the monolithic integration of silicon very large scale integration (VLSI) electronics with Si nanophotonics on a single silicon chip in a commercial state-of-the-art CMOS SOI production plant Soref (2006). The serious challenge of the Si based photonic integrated circuit is the fabrication of Si-based, electrically pumped light-emitting devices (LEDs) since Si possesses an indirect band gap with a low probability for radiative electron-hole recombination Reed (2004). In order to prevent carrier diffusion to nonradiative centres the low-dimensional structures such as porous silicon, nano-crystals, Er-doped nano-crystals have been proposed Reed (2004). The performance of light-emitting devices based on the crystalline, amorphous and Er-doped Si nanostructures has been investigated, and a stable electroluminescence (EL) at $850nm$ and $1.54\mu m$ has been demonstrated Iacona (2006). Si QDs embedded in the silicon nitride thin films may provide an alternative possibility for a Si-based full-color emission Sung (2006). Still, the electrical carrier injection and the efficient extraction of the emitted are the main obstacles for the fabrication of the highly efficient Si based LED Sung (2006).
Recently, InGaAs QD lasers on Si have been developed and monolithically integrated with crystalline and amorphous Si waveguides and InGaAs quantum well (QW) electroabsorption modulators (EAM) Mi (2009). The measured threshold current for such QD lasers is still much larger than that of QD lasers grown on GaAs. However, under certain technological conditions, the performance of QD lasers on Si may be essentially improved, and the characteristics comparable to the QD lasers grown on GaAs substrates can be achieved Mi (2009). Then, the high performance 1.3 and $1.55\mu m$ QD lasers on Si can be realized Mi (2009). In the framework of an integrated all-optical signal processing system, such an externally or directly modulated QD laser can be used as a source of UWB modulated optical carriers. Integrated UMZIs based on Si waveguides can then generate UWB Gaussian monocycles and doublets.
Taking into account the unique possibilities of the Si photonic integrated circuits combined with InGaAs QD lasers we may predict the essential improvement of the UWB optical links based on such devices. We used the QD laser rate equations and investigated theoretically the direct modulation of QD laser radiation and its influence on the optical link performance.

7. QD Lasers

In this section we briefly describe the structure and optical properties of QDs. Then, we discuss the QD laser dynamic model based on the coupled rate equations for carrier population. We present the original results based on the numerical simulations for the analog optical link containing a QD laser.

7.1 QD Structure

Quantization of electron states in all three dimensions results in a creation of a novel physical object - a macroatom, or QD containing a zero dimensional electron gas. Size quantization is effective when the QD three dimensions are of the same order of magnitude as the electron de Broglie wavelength which is about several nanometers Ustinov (2003). QD is a nanomaterial confined in all the three dimensions, and for this reason it has unique electronic and optical properties that do not exist in bulk semiconductor material Ohtsu (2008). An electron-hole pair created by light in a QD has discrete energy eigenvalues caused by the electron-hole

confinement in the material. This phenomenon is called a quantum confinement effect Ohtsu (2008).
The different types of QDs based on different technologies and operating in different parts of spectrum are known such as In(Ga)As QDs grown on GaAs substrates, InAs QDs grown on InP substrates, and colloidal free-standing InAs QDs. QD structures are commonly realized by a self-organized epitaxial growth where QDs are statistically distributed in size and area. A widely used QDs fabrication method is a direct synthesis of semiconductor nanostructures based on the island formation during strained-layer heteroepitaxy called the Stranski-Krastanow (SK) growth mode Ustinov (2003). The spontaneously growing QDs are said to be self-assembling. SK growth has been investigated intensively for InAs on GaAs, InP on GaInP, and Ge on Si structures Ustinov (2003). The energy shift of the emitted light is determined by size of QDs that can be adjusted within a certain range by changing the amount of deposited QD material. Evidently, smaller QDs emit photons of shorter wavelengths Ustinov (2003).
The simplest QD models are described by the spherical boundary conditions for an electron or a hole confinement in a spherical QD with a radius R, or by the cubic boundary conditions for a parallelepiped QD with a side length $L_{x,y,z}$ Ohtsu (2008). In the first case, the electron and hole energy spectra $E_{e,nlm}$ and $E_{h,nlm}$ are given by, respectively Ohtsu (2008)

$$E_{e,nlm} = E_g + \frac{\hbar^2}{2m_e}\left(\frac{\alpha_{nl}}{R}\right)^2; E_{h,nlm} = \frac{\hbar^2}{2m_h}\left(\frac{\alpha_{nl}}{R}\right)^2 \tag{16}$$

where

$$n = 1, 2, 3, ...; l = 0, 1, 2, ...n-1; m = 0, \pm 1, \pm 2, .. \pm l \tag{17}$$

E_g is the QD semiconductor material band gap, $m_{e,h}$ are the electron and hole effective mass, respectively, $\hbar = h/2\pi$, h is the Planck constant, and α_{nl} is the n-th root of the spherical Bessel function. In the second case, the energy eigenvalues $E_{e,nlm}$ and $E_{h,nlm}$ are given by, respectively Ohtsu (2008)

$$E_{e,nlm} = E_g + \frac{\hbar^2\pi^2}{2m_e}\left[\left(\frac{n}{L_x}\right)^2 + \left(\frac{l}{L_y}\right)^2 + \left(\frac{m}{L_z}\right)^2\right] \tag{18}$$

$$E_{h,nlm} = \frac{\hbar^2\pi^2}{2m_h}\left[\left(\frac{n}{L_x}\right)^2 + \left(\frac{l}{L_y}\right)^2 + \left(\frac{m}{L_z}\right)^2\right]$$

The density of states (DOS) $\rho_{QD}(E)$ for an array of QDs has the form Ustinov (2003)

$$\rho_{QD}(E) = \sum_n \sum_m \sum_l 2n_{QD}\delta\left(E - E_{e,nlm}\right) \tag{19}$$

where $\delta\left(E - E_{e,nlm}\right)$ is the δ-function, and n_{QD} is the surface density of QDs.
Detailed theoretical and experimental investigations of InAs/GaAs and InAs QDs electronic structure taking into account their more realistic lens, or pyramidal shape, size, composition profile, and production technique (SK, colloidal) have been carried out Bimberg (1999), Bányai (2005), Ustinov (2003). A system of QDs can be approximated with a three energy level model in the conduction band containing a spin degenerate ground state GS, fourfold degenerate excited state (ES) with comparatively large energy separations of about $50 - 70meV$, and a narrow continuum wetting layer (WL). The electron WL is situated $150meV$ above the lowest electron energy level in the conduction band, i.e. GS and has a width of approximately

$120meV$. In real cases, the QDs vary in size, shape, and local strain which leads to the fluctuations in the quantized energy levels and the inhomogeneous broadening in the optical transition energy. The QDs and WL are surrounded by a barrier material which prevents direct coupling between QD layers. The absolute number of states in the WL is much larger than in the QDs. GS and ES in QDs are characterized by homogeneous and inhomogeneous broadening Bányai (2005). The homogeneous broadening caused by the scattering of the optically generated electrons and holes with imperfections, impurities, phonons, or through the radiative electron-hole pair recombination Bányai (2005) is about $15meV$ at room temperature. The eigenspectrum of a single QD fully quantized in three dimensions consists of a discrete set of eigenvalues depending only on the number of atoms in it. Variations of eigenenergies from QD to QD are caused by variations of QD's strain and shape. The finite carrier lifetime results in Lorentzian broadening of a finite width Ustinov (2003). The optical spectrum of QDs consists of a series of transitions between the zero-dimensional electron gas energy states where the selections rules are determined by the form and symmetry of QDs Ustinov (2003). In(Ga)As/GaAs QDs are characterized by emission at wavelengths no longer than $\lambda = 1.35\mu m$, while the InAs/InP QDs have been proposed for emission at the usual telecommunication wavelength $\lambda = 1.55\mu m$ Ustinov (2003).

7.2 Dynamics of QD Lasers

Fabrication techniques, structure, electrical and optical properties as well as possible applications of QD lasers have been thoroughly investigated Ustinov (2003), Ledentsov (2008), Mi (2009). QD lasers based on self-organized InGaN, InAs, InGaAlP nanostructures have been proposed for different applications from the ultraviolet (UV) to the far infrared (IR) spectral range Ledentsov (2008). They demonstrate extremely low threshold current densities, high temperature stability, potential low wavelength chirp, fast carrier dynamics, and modified DOS function which should lead to the improved performance Ustinov (2003), Thompson (2009). In particular, the InAs/GaAs QD lasers based on 3-D nanometer scale islands with dimensions of about $10nm$ are promising in fiber optic applications in the $1.3\mu m$ wavelength range. QD edge-emitting lasers and VCSELs can be realized Ustinov (2003), Ledentsov (2008). In UWB optical link applications the QD laser direct modulation is essential. The detailed study of QD laser dynamics is necessary for the evaluation of signal dispersion, modulation-induced chirping, linewidth, etc. Tan (2009). Modulation characteristics of QD lasers are limited by small area density of QDs grown by SK technique and the inhomogeneous gain broadening caused by the QD size fluctuations Sakamoto (2000), Sugawara (2002), Sugawara (2004), Ledentsov (2008). A Gaussian distribution may be used for the description of the QD sizes, and it shows that the discrete resonances merge into a continuous structure with widths around 10% Bányai (2005). The ensemble of QDs should be divided into groups by their resonant frequency of the GS transition between the conduction and valence bands Sugawara (2002), Sugawara (2004). However, in some cases the gain broadening is desirable providing a stable VCSEL operation in a wide temperature range Ledentsov (2008). It may be also helpful in the case of single-source multichannel data transmission systems Ledentsov (2008). It has been shown theoretically that the inhomogeneous broadening in QD SOA limits the pulse duration to nanoseconds or even several dozen picoseconds for a large enough bias current Ben Ezra (2007). Unlike bulk and QW lasers, the modulation bandwidth in QD lasers is essentially determined by the carrier relaxation and radiative recombination due to the complete quantization of the energy levels Chow (2005).

The analysis of QD laser dynamic behavior can be derived from the phenomenological rate equations, or from quantum mechanical theories. A semiclassical approach is based on the laser field and active medium description by the Maxwell-Bloch equations which account for nonequilibrium effects on time scales from subpicosecond to nanoseconds Chow (2005). This microscopic approach is extremely complicated due to a large number of effects to be included in general case.
The alternative phenomenological approach based on the coupled rate equation system for the carriers is widely used both for QD lasers and for QD SOAs Berg (2001), Berg (2004), Berg (November 2004), Ben Ezra (September 2005), Ben Ezra (October 2005), Ben Ezra (2007), Ben Ezra (2008), Qasaimeh (2003), Qasaimeh (2004), Sakamoto (2000), Uskov (2004), Yavari (2009), Tan (2009), Kim (2009). Typically, the electron-hole pair is considered as a one bound state, or an exciton, and only the carrier dynamics in conduction band is investigated. Recently, a more complicated model has been proposed for QD SOA where the dynamics of electrons and holes has been considered separately Kim (2009).
We use the standard approach where the hole dynamics is neglected. The QD laser model includes WL, upper continuum state (CS), GS and ES where the carriers are injected into WL, then they relax to CS serving as a carrier reservoir, and finally to GS and ES in each QD ensemble Yavari (2009), Tan (2009). The energy band structure of the QD laser is shown in Fig. 11.

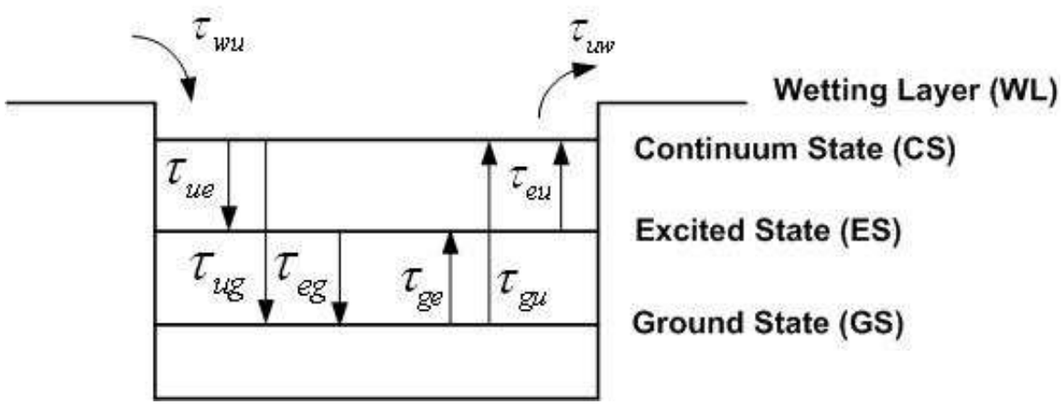

Fig. 11. The energy band structure of a QD laser

Carrier thermal emission occurs among CS, ES, and GS, and separately, between CS and WL Tan (2009). The stimulated emission of photons occurs above the threshold bias current due to the carrier transitions from GS Yavari (2009), Tan (2009). The system of the coupled rate equations has the form Tan (2009).

$$\frac{dN_w}{dt} = \frac{\eta_i I}{q} - \frac{N_w}{\tau_{wr}} - \frac{N_w}{\overline{\tau}_{wu}} + \frac{1}{\tau_{uw}} \sum_j N_{u,j} \tag{20}$$

$$\frac{dN_{u,j}}{dt} = \frac{N_w G_n}{\tau_{wu,j}} + \frac{N_{g,j}}{\tau_{gu,j}} + \frac{N_{e,j}}{\tau_{eu,j}} - \frac{N_{u,j}}{\tau_{ug,j}} - \frac{N_{u,j}}{\tau_{ue,j}} - \frac{N_{u,j}}{\tau_{uw}} - \frac{N_{u,j}}{\tau_r} - \frac{c\Gamma}{n_r} \sum_m g_{mn} S_m \tag{21}$$

$$\frac{dN_{e,j}}{dt} = \frac{N_{u,j}}{\tau_{ue,j}} + \frac{N_{g,j}}{\tau_{ge,j}} - \frac{N_{e,j}}{\tau_{eu,j}} - \frac{N_{e,j}}{\tau_{eg,j}} - \frac{N_{e,j}}{\tau_r} - \frac{c\Gamma}{n_r}\sum_m g_{mn}S_m \tag{22}$$

$$\frac{dN_{g,j}}{dt} = \frac{N_{u,j}}{\tau_{ug,j}} + \frac{N_{e,j}}{\tau_{eg,j}} - \frac{N_{g,j}}{\tau_{gu,j}} - \frac{N_{g,j}}{\tau_{ge,j}} - \frac{N_{g,j}}{\tau_r} - \frac{c\Gamma}{n_r}\sum_m g_{mn}S_m \tag{23}$$

Here I is the current injection, η_i is the internal quantum efficiency, q is the electron charge, the subscript j refers to the jth group of QDs, the subscripts w, u, e and g refer to WL, CS, ES and GS, respectively; N_w, $N_{u,j}$, $N_{e,j}$, $N_{g,j}$ are the carrier populations in the WL, CS, ES, and GS of the jth QD group, respectively; S_m is the number of photons in the mth mode, c is the free space light velocity, Γ is the optical confinement factor, g_{mn} is the linear optical gain of the nth QD group contributing to the mth mode photons, τ_{wr} is the recombination lifetime constant in the WL, $\overline{\tau}_{wu}$ is the average carrier relaxation time from WL to CS, τ_r is the common recombination lifetime in each group of QDs, τ_{uw} is the excitation lifetime from CS to WL. The total active region volume V_A is given by Tan (2009).

$$V_A = HdLn_w \tag{24}$$

where H is the QD height, L is the laser cavity length, d is the width of the device, n_w is the number of dot layers in the active region.

7.3 Direct Modulation of QD Lasers by UWB Signals in an Analog Optical Link

In order to investigate the performance of the analog optical link containing a QD laser, we have carried out the numerical simulations of the QD laser direct modulation in the MB OFDM case using rate equations (20)-(23). The typical values of the essential device parameters used in our simulations are similar to the ones used in Refs. Yavari (2009), Tan (2009). For instance, a WL thickness is $1nm$, $L = 800\mu m$, the volume density of QDs is $N_D = 1.67 \times 10^{23} m^{-3}$, the volume of active region is $9.6 \times 10^{-16} m^3$, $\overline{\tau}_{wu} = 1ps$, $\tau_{uw} = 10ps$, $\tau_{wr} = 0.4ns$, $\tau_r = 1ns$, spontaneous emission lifetime $2.8ns$. The QD laser is biased with the dc current $I = 10mA$ and MB OFDM UWB signal at the power level of $-14dBm$. The resulting modulated optical signal in shown in Fig. 12. The corresponding spectra of the modulated bandpass and baseband

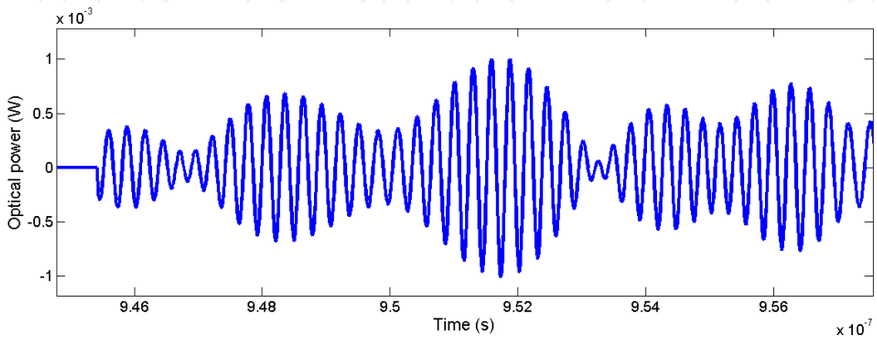

Fig. 12. Directly modulated optical power of the QD laser in the analogous optical link

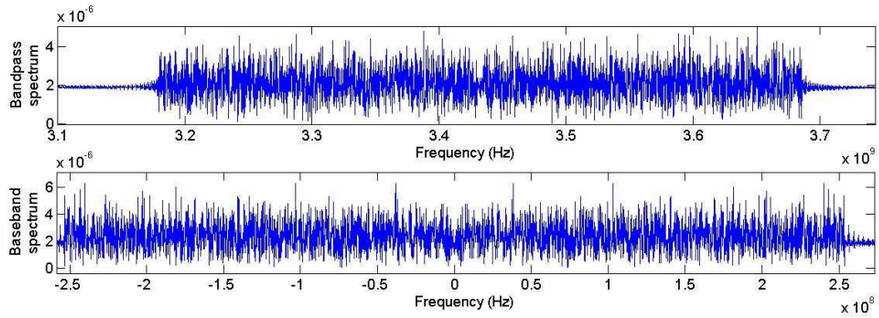

Fig. 13. Spectrum of the directly modulated QD laser radiation (upper box); spectrum of the baseband signal (lower box)

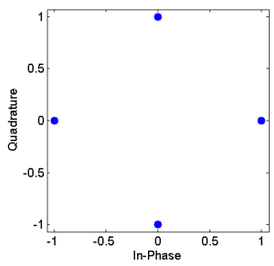

Fig. 14. Constellation diagram of the signal transferred through the analogous optical link

signals are shown in Fig. 13. The modulated signal was transmitted over SMF of a $1km$ length and detected with a photodiode (PD). The responsivity of PD was $R = 0.95A/W$ and the radio frequency bandwidth was $10GHz$. The constellation diagram of the received baseband UWB signal is shown in Fig. 14. The constellation diagram clearly shows the high quality of the transmission over the optical link containing QD laser which corresponds to the non-distorted form of the optical signal and its spectrum.

8. Conclusions

We have discussed state-of-the-art of the UWB communications, the novel trends such as UROOF technology, theoretical and experimental results for the photonic generation of UWB pulses, the importance of the high level integration of novel photonic and electronic components for UWB communications, and applications of QD lasers and QD SOAs. The integration of QD lasers with the Si photonics on a Si platform can significantly improve the performance of UWB communication systems and reduce the cost. We have carried out the numerical simulations for the analog optical link containing the QD laser. The performance of the optical link is significantly improved due to high linearity, large bandwidth and low noise of the QD laser. Further detailed theoretical and experimental investigations in the field of QD devices are required in order to develop new generations of UWB communication systems mainly based on the all-optical signal processing.

9. References

Agrawal, G.P. (2002). *Fiber-Optic Communication Systems*. Wiley, ISBN 0-471-21571-6, New York

Armstrong, J. (2009). OFDM for Optical Communications, *IEEE Journal of Lightwave Technology*, Vol. 27, No. 3 (February 2009) 189-204, ISSN 0733-8724

Bányai, L. & Koch, S. W. (2005). *Semiconductor Quantum Dots* (Second Edition). World Scientific, ISBN 9810213905, London

Ben-Ezra, Y.; Haridim, M. & Lembrikov, B. I. (2005). Theoretical analysis of gain-recovery time and chirp in QD-SOA. *IEEE Photonics Technology Letters*, Vol. 17, No. 9, (September 2005) 1803-1805, ISSN 1041-1135

Ben-Ezra, Y.; Lembrikov, B. I. & Haridim, M. (2005). Acceleration of gain recovery and dynamics of electrons in QD-SOA. *IEEE Journal of Quantum Electronics*, Vol. 41, No. 10, (October 2005) 1268-1273, ISSN 0018-9197

Ben-Ezra, Y.; Lembrikov, B. I. & Haridim, M. (2007). Specific features of XGM in QD-SOA. *IEEE Journal of Quantum Electronics*, Vol.43, No. 8, (August 2007) 730-737, ISSN 0018-9197

Ben Ezra, Y.; Haridim, M.; Lembrikov, B.I. & Ran, M. (2008). Proposal for All-optical Generation of Ultra Wideband Impulse Radio Signals in Mach-Zehnder Interferometer with Quantum Dot Optical Amplifier. *IEEE Photonics Technology Letters*, Vol. 20, No. 7 (April 2008) 484-486, ISSN 1041-1135

Ben Ezra, Y.; Lembrikov, B.I.; Ran, M. & Haridim, M. (2009). All Optical Generation and Processing of IR UWB Signals", In: *Optical Fibre, New Developments*. Christophe Lethien (Ed.), In-Tech, 2009, Vukovar, Croatia, pp. 425-444, ISBN 978-953-7619-50-3

Ben Ezra, Y. & Lembrikov, B.I. (June 2009). Optical wavelet signal processing. *11th Int'l. Conf. on Transparent Optical Networks (ICTON 2009).* Azores, Portugal, 28 June-2 July 2009, We. A.2.2, pp. 1-4, ISBN 978-1-4244-4826-5

Berg, T.W.; Bischoff, S.; Magnusdottir, I. & Mørk, J. (2001). Ultrafast gain recovery and modulation limitations in self-assembled quantum-dot devices. *IEEE Photonics Technology Letters*, Vol. 13, No. 6 (June 2001) 541-543, ISSN 1041-1135

Berg, T.W.; Mørk, J. & Hvam, J.M. (2004). Gain dynamics and saturation in semiconductor quantum dot amplifiers. *New Journal of Physics*, Vol. 6, No. 178, (2004) 1-23, ISSN 1367-2630

Berg, T.W. & Mørk, J. (2004). Saturation and Noise Properties of Quantum-Dot Optical Amplifiers. *IEEE J. of Quantum Electronics*, Vol. 40, No. 11, (November 2004) 1527-1539, ISSN 0018-9197

Bimberg, D.; Grundmann, M. & Ledentsov, N. N. (1999). *Quantum Dot Heterostructures*. John Wiley, ISBN 047 1973882, New York

Chong, C.-C.; Watanabe, F. & Inamura, H. (2006). Potential of UWB technology for the next generation wireless communications. *Proceedings of 2006 IEEE Ninth International symposium on Spread Spectrum Techniques and Applications, Manaus, Amazon, Brazil* (28-31 August 2006) 422-429, ISBN 0-7803-9779-7

Chow, W.W. & Koch, S. W. (2005). Theory of semiconductor quantum-dot laser dynamics. *IEEE J. of Quantum Electronics*, Vol. 41, No. 4, (April 2005) 495-505, ISSN 0018-9197

Cox, III, C.H. (2003). Analog optical links: models, measures and limits of performance. In: *Microwave Photonics* Vilcot, A., Cabon, B. & Chazelas, J. (Eds.), 210-219, Kluver, ISBN 1-4020-7362-3, Boston

Ghavami, M.; Michael, L.B. & Kohno, R. (2005). *Ultra Wideband Signals and Systems in Communication Engineering*, Wiley, ISBN-10 0-470-86571-5(H/B), Chichester, England

Iacona, F.; Irrera, A.; Franzò, G.; Pacifici, D.; Crupi, I.; Miritello, M.; Presti, C.D. & Priolo, F. (2006). Silicon-based light-emitting devices: properties and applications of crystalline, amorphous and Er-doped nanoclusters. *IEEE Journal of Selected Topics in Quantum Electronics*, Vol. 12, No. 6 (November/December 2006) 1596–1606, ISSN 1077-260X

Jalali, B. & S. Fathpour, S. (2006). Silicon Photonics, *Journal of Lightwave Technology,* Vol.24, No. 12, (December 2006) 4600-4615, ISSN 0733-8724

Kim, J.; Laemmlin, M.; Meuer, C.; Bimberg, D. & Eisenstein, G. (2009). Theoretical and experimental study of high-speed small-signal cross-gain modulation of quantum-dot semiconductor optical amplifiers. *IEEE J. of Quantum Electronics*, Vol. 45, No. 3, (March 2009) 240-248, ISSN 0018-9197

Kshetrimayum, R. S. (2009). An Introduction to UWB Communication Systems. *Potentials, IEEE*, Vol. 28, Issue 2, (March-April 2009) 9-13, ISSN 0278-6648

Ledentsov, N.N.; Bimberg, D. & Alferov, Zh.I. (2008). Progress in epitaxial growth and performance of quantum dot and quantum wire lasers, *Journal of Lightwave Technology,* Vol.26, No. 11, (June 2006) 1540-1555, ISSN 0733-8724

Le Guennec, Y. & Gary, R. (2007). Optical frequency conversion for millimeter-wave ultra-wideband-over-fiber systems. *IEEE Photonics Technology Letters,* Vol. 19, No. 13, (July 2007) 996-998, ISSN 1041-1135

Lin, W.-P. & Chen, J.-Y. (2005). Implementation of a new ultrawide-band impulse system, *IEEE Photonics Technology Letters*, Vol. 17, No. 11, (November 2005) 2418-2420, ISSN 1041-1135

Mi, Z.; Yang, J.; Bhattacharya, P.; Qin, G. & Ma, Z. (2009). High-Performance quantum dot lasers and integrated optoelectronics on Si. *Proceedings of the IEEE*, Vol. 97, No. 7, (July 2009) 1239-1249, ISSN 0018-9219

Ohtsu, N.; Kobayashi, K.; Kawazoe, T.; Yatsui, T. & Naruse, N. (2008). *Principles of Nanophotonics,* CRC Press, ISBN-13 978-1-58488-972-4, London

Qasaimeh, O. (2003). Optical gain and saturation characteristics quantum-dot semiconductor optical amplifiers. *IEEE J. of Quantum Electronics*, Vol. 39, No. 6, (June 2003) 793-798, ISSN 0018-9197

Qasaimeh, O. (2004). Characteristics of cross-gain (XG) wavelength conversion in quantum dot semiconductor optical amplifiers. *IEEE Photonics Technology Letters*, Vol. 16, No. 2, (February 2004) 542-544, ISSN 1041-1135

Qui, R. C.; Shen, X.; Guizani, M. & Le-Ngoc, T. (2006). Introduction, In: *Ultra-wideband wireless communications and networks,* Shem, X., Guizani, M., Qui, R. C., Le-Ngoc, T. (Ed.), 1-14, Wiley, ISBN 0-470-01144-0, Chichester, England

Ran, M; Ben Ezra, Y. & Lembrikov B.I. (2009). Ultra-wideband Radio-over-optical-fibre Technologies, In: *Short-Range Wireless Communications*, Kraemer, R. & Katz, M. D. (Eds.), 271-327, Wiley, ISBN 978-0-470-69995-9 (H/B), Chichester, England

R.M. Rao and A.S. Bopardikar (1998). *Wavelet Transforms. Introduction to Theory and Applications*. Addison-Wesley, Addison-Wesley, ISBN-10: 020 16 34 635, Reading, Massachusetts

Reed, G.T. & Knights, A.P. (2004). *Silicon Photonics,* Wiley, ISBN 0-470-87034-6, Chichester, England

Sakamoto, A. & Sugawara, M. (2000). Theoretical calculation of lasing spectra of quantum-dot lasers: effect of homogeneous broadening of optical gain, *IEEE Photonics Technology Letters*, Vol. 12, No. 2, (February 2000) 107-109, ISSN 1041-1135

Shieh, W.; Bao, H. & Tang, Y. (2008). Coherent optical OFDM: theory and design. *Optics Express*, Vol.16, No. 2, (January 2008) 841-859, ISSN 1094-4087

R. Soref, R. (2006). The Past, present, and future of Si photonics, *IEEE Journal of Selected Topics in Quantum Electronics,* Vol.13, No. 6, (November/December 2006) 1678-1687, ISSN 1077-260X

Sugawara, M.; T. Akiyama, T.; N. Hatori, N. ; Y. Nakata, Y.; Ebe, H. & H. Ishikava, H. (2002). Quantum-dot semiconductor optical amplifiers for high-bit-rate signal processing up to 160 Gbs^{-1} and a new scheme of 3R regenerators, *Meas. Sci. Technol.*, Vol. 13, (2002), 1683-1691, ISSN 0957-0233

Sugawara, M.; Ebe, H.; Hatori, N.; Ishida, M.; Arakawa, Y.; Akiyama, T.; Otsubo, K. & Nakata, Y. (2004) Theory of optical signal amplification and processing by quantum-dot semiconductor optical amplifiers. *Phys. Rev.B,* Vol. 69, No. 23 (June 2004) 235332-1-39, ISSN 1098-0121

Sung, G.Y. & al (2006). Physics and device structures of highly efficient silicon quantum dots based silicon nitride light-emitting diodes. *IEEE Journal of Selected Topics in Quantum Electronics*, Vol. 12, No. 6 (November/December 2006) 1545–1555, ISSN 1077-260X

Tan, C. L.; Wang, Y.; Djie, H. S. & Ooi, B. S. (2009). The dynamic characteristics and linewidth enhancement factor of quasi-supercontinuum self-assembled quantum dot laser, *IEEE Journal of Quantum Electronics*, Vol. 45, No. 9, (September 2009) 1177-1182, ISSN 0018-9197

Thompson, M.G.; Rae, A.R.; Xia, M.; Penty, R.V. & White, I.H. (2009). InGaAs quantum-dot mode-locked laser diodes. *IEEE Journal of Selected Topics in Quantum Electronics*, Vol. 15, No. 3 (May/June 2009) 661–672, ISSN 1077-260X

Uskov, A.V. ; Berg, T.W. & Mørk, J. (2004). Theory of pulse-train amplification without patterning effects in quantum-dot semiconductor optical amplifiers. *IEEE J. of Quantum Electronics*, Vol. 40, No. 3, (March 2004) 306-320, ISSN 0018-9197

Ustinov, V.M.; Zhukov, A.E.; Egorov, A. Yu. & Maleev, N. A. (2003). *Quantum Dot Lasers,* Oxford University Press, ISBN 0 19 852679 2, Oxford

Wada, O. (2007). Femtosecond all-optical devices for ultrafast communication and signal processing, In: *Microwave Photonics,* Lee, C. H. (Ed), 31-75, CRC Press, ISBN-10: 0-8493-3924-3

Wang, Q. & Yao, J. (2006). UWB doublet generation using nonlinearly-biased electro-optic intensity modulator, *Electronic Letters*, Vol. 42, No. 22, (October 2006)1304-1305, ISSN 0013-5194

Yang, L. & Giannakis, G.B. (2004). Ultra-Wideband Communications. *IEEE Signal Processing Magazine*, Vol. 21, No. 6; (November 2004) 26-54, ISSN 1053-5888

Yao, J.; Zeng, F. & Wang, Q. (2007). Photonic generation of ultrawideband signals. *Journal of Lightwave Technology,* Vol. 25, No. 11, (November 2007) 3219-3235, ISSN 0733-8724

Yao, J. (2009). Photonics for ultrawideband communications, *IEEE Microwave Magazine,* Vol. 10, No. 4, (June 2009) 82-95, ISSN 1527-3342

Yavari, M.H. & Ahmadi, V. (2009). Circuit-level implementation of semiconductor self-assembled quantum dot laser. *IEEE Journal of Selected Topics in Quantum Electronics*, Vol. 15, No. 3 (May/June 2009) 774–779, ISSN 1077-260X

Zeng, F. & Yao, J. (2006). An approach to ultrawideband pulse generation and distribution over optical fiber. *IEEE Photonics Technology Letters*, Vol. 18, No. 7, (April 2006) 823-825, ISSN 1041-1135

Zeng, F. & Yao, J. (2006). Ultrawideband impulse radio signal generation using a high-speed electrooptic phase modulator and a fiber-Bragg-grating-based frequency discriminator. *IEEE Photonics Technology Letters,* Vol. 18, No. 19, (October 2006) 2062-2064, ISSN 1041-1135

Zeng, F.; Wang, O. & Yao, J.P. (2007). All-optical UWB impulse generation based on cross-phase modulation and frequency discrimination. *Electronic Letters,* Vol. 43, No. 2, (January 2007) 119-121, ISSN 0013-5194

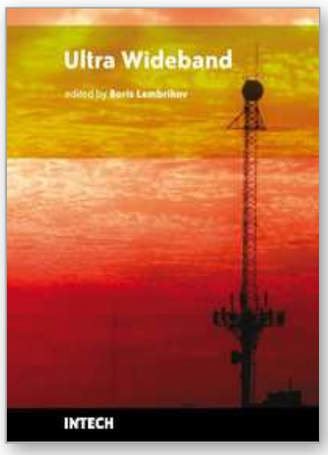

Ultra Wideband

Edited by Boris Lembrikov

ISBN 978-953-307-139-8

Hard cover, 458 pages

Publisher Sciyo

Published online 17, August, 2010

Published in print edition August, 2010

Ultra wideband technology is one of the most promising directions in the rapidly developing modern communications. Ultra wideband communication system applications include radars, wireless personal area networks, sensor networks, imaging systems and high precision positioning systems. Ultra wideband transmission is characterized by high data rate, availability of low-cost transceivers, low transmit power and low interference. The proposed book consisting of 19 chapters presents both the state-of-the-art and the latest achievements in ultra wideband communication system performance, design and components. The book is addressed to engineers and researchers who are interested in the wide range of topics related to ultra wideband communications.

How to reference

In order to correctly reference this scholarly work, feel free to copy and paste the following:

Yosef Ben-Ezra, Boris Lembrikov and Moshe Ran (2010). High Performance Analog Optical Links Based on Quantum Dot Devices for UWB Signal Transmission, Ultra Wideband, Boris Lembrikov (Ed.), ISBN: 978-953-307-139-8, InTech, Available from: http://www.intechopen.com/books/ultra-wideband/high-performance-analog-optical-links-based-on-quantum-dot-devices-for-uwb-signal-transmission

INTECH
open science | open minds

InTech Europe
University Campus STeP Ri
Slavka Krautzeka 83/A
51000 Rijeka, Croatia
Phone: +385 (51) 770 447
Fax: +385 (51) 686 166
www.intechopen.com

InTech China
Unit 405, Office Block, Hotel Equatorial Shanghai
No.65, Yan An Road (West), Shanghai, 200040, China
中国上海市延安西路65号上海国际贵都大饭店办公楼405单元
Phone: +86-21-62489820
Fax: +86-21-62489821

IntechOpen